

RESEARCH ARTICLE



## An adaptive method based on the improved LPA-ICI algorithm for MRI enhancement

Jonatan Lerga , Ivica Mandić, Hajdi Peić and Dražen Brščić

Faculty of Engineering, Department of Computer Engineering, University of Rijeka, Rijeka, Croatia

### ABSTRACT

Various diseases are diagnosed using medical imaging used for analysing internal anatomical structures. However, medical images are susceptible to noise introduced in both acquisition and transmission processes. We propose an adaptive data-driven image denoising algorithm based on an improvement of the intersection of confidence intervals (ICI), called relative ICI (RICI) algorithm. The 2D mask of the adaptive size and shape is calculated for each image pixel independently, and utilized in the design of the 2D local polynomial approximation (LPA) filters. Denoising performances, in terms of the PSNR, are compared to the original ICI-based method, as well as to the fixed sized filtering. The proposed adaptive RICI-based denoising outperformed the original ICI-based method by up to 1.32 dB, and the fixed size filtering by up to 6.48 dB. Furthermore, since the denoising of each image pixel is done locally and independently, the method is easy to parallelize.

### ARTICLE HISTORY

Received 24 January 2018  
Accepted 4 June 2018

### KEYWORDS

Adaptive filtering;  
intersection of confidence  
intervals; relative intersection  
of confidence intervals; local  
polynomial approximation;  
image enhancement; image  
denoising; medical imaging;  
magnetic resonance imaging

## Introduction

Since its introduction in 1973, magnetic resonance imaging (MRI) led to revolutionary discoveries in bio-medical applications, especially in medical diagnostics [1]. Today, MRIs are commonly used in medical radiology for capturing images of internal human anatomy and physiological processes in search for possible diseases [2]. However, recorded images are usually of low quality requiring some numerical processing for improving their readability. Artefacts in MRIs are often caused by patient movements (which result in distortions in the captured data similar to blurring of photographs), metal implants (which affect magnetic fields in their vicinity causing dark patches or shadows in the recorded images) and noise (which blurs edges of adjacent soft tissues) [3].

Furthermore, MRI images, as well as X-ray images, are often of low contrast and high homogeneity [4]. In order to improve image contrast, X-ray images require patient exposures to higher radiation doses. On the other hand, the price paid to improve MRI image contrast is imaging time [4]. Furthermore, there is also a compromise between image contrast and noise level, as well as blurring of MRIs. Namely, when selecting a certain imaging method, one has to specify the maximal acceptable noise level and adjust other imaging factors in order to achieve them with minimum exposure, imaging time and effect on other image characteristics [4].

In general, noise in MRIs is often caused by radiofrequency pulses, radiofrequency coil, field strength, voxel volume and/or receiver bandwidth [5]. It may

significantly reduce the reliability of MRIs leading to possible misinterpretations and incorrect diagnoses, thus, denoising preprocessing (such that tissue contours and textures are preserved while the noise is smoothed) is an important requirement preceding their analysis (such as MRI segmentation and pattern recognition).

MRI denoising approaches are either acquisition-based noise reduction or post-acquisition based image filtering. The first approaches are based on hardware improvements often resulting in an increase of image capturing duration or reduction of spatial resolution. Thus, post-acquisition image improvement is often the only way to achieve the desired MRI quality [6,7]. The post-acquisition MRI denoising methods may be divided into linear and non-linear filtering methods. Linear methods, for instance, estimate noise-free pixel values by weighted averaging of the pixels in the vicinity of the considered pixel. Unfortunately, smoothing the noise often leads to degrading other image characteristics, such as object edges. On the other hand, non-linear methods often outperform linear methods in preserving object edges while degrading fine image structures [5].

This paper proposes an adaptive method for MRI image denoising based on 2D spatial filters designed using the local polynomial approximation (LPA) and the improved intersection of confidence intervals (ICI) algorithm called the relative intersection of confidence intervals (RICI) algorithm. The data-driven LPA-RICI method has been shown to perform well in noise-

free pixel estimation since the RICl algorithm detects near optimal size and shape of the 2D vicinity neighbouring the considered pixel [8,9]. The detected 2D regions are then utilized as binary masks for MRI image segmentation and estimation of the noise-free pixel value by applying LPA weighted filtering to the extracted regions. Owing to its adaptivity to local image content, the proposed denoising method was shown to efficiently suppress additive noise and, at the same time, preserve tissues contours and borders avoiding blurring artefacts. The procedure is repeated independently for each pixel. Hence, the computational efficiency of MRI denoising can be easily improved by parallelized implementation of the proposed method.

The proposed 2D LPA-RICl method was tested on real-life MRI images outperforming the original ICI based method and other fixed size filtering methods.

The paper is organized as follows. Section 2 presents the original ICI rule and its improvement (the RICl rule) extended to 2D image processing. Section 3 gives the experimental results for tested medical images, as well as detailed elaboration on the achieved results. The conclusion is found in Section 4.

## The ICI rule and its improvement

### The ICI rule

This section presents the original one-dimensional ICI algorithm and its novel modification called the RICl algorithm, both upgraded to process two-dimensional images.

For each signal sample  $n$ , the one-dimensional LPA-ICI method introduces a set of  $K$  estimators  $H$  with an increasing size  $h_k$  [8,9]:

$$H = \{h_1 < h_2 < \dots < h_K\}, \quad (1)$$

and a corresponding set of confidence intervals:

$$D_{h_k}(n) = [L_k(n), U_k(n)], \quad (2)$$

where  $1 \leq k \leq K$ . Upper  $U_{h_k}$  and lower  $L_{h_k}(n)$  limits of the confidence interval are defined as [8,9]:

$$U_{h_k}(n) = \hat{y}_{h_k}(n) + \Gamma \sigma_{h_k}(n), \quad (3)$$

$$L_{h_k}(n) = \hat{y}_{h_k}(n) - \Gamma \sigma_{h_k}(n), \quad (4)$$

where parameter  $\Gamma$  defines the confidence level,  $\sigma_{h_k}(n)$  stands for the standard deviation of the estimation error, and  $\hat{y}_{h_k}(n)$  is calculated as the LPA weighted average of  $k$  samples neighbouring the considered sample [8,9].

Next, the ICI rule tracks the values of the smallest upper and the largest lower confidence intervals limits [8,9]:

$$\underline{U}_{h_k}(n) = \min_{i=1, \dots, k} U_{h_i}(n), \quad (5)$$

$$\bar{L}_{h_k}(n) = \max_{i=1, \dots, k} L_{h_i}(n), \quad (6)$$

as long as the following criterion is met:

$$\bar{L}_{h_k}(n) \leq U_{h_k}(n), \quad (7)$$

Namely, confidence intervals are calculated as long as all previous  $k$  intervals are overlapping (or until the end of the signal is reached). Finally, the optimal estimator size is determined as the largest  $k$  for which all previous confidence intervals, including  $k$ -th interval, are overlapping [8,9].

As demonstrated in [10], estimate error variance is increased by small  $h_k$  values and, at the same time, the estimation error bias is decreased. On the other hand, large  $h_k$  values result in a decreasing estimate error variance and an increase of its bias [10]. The aforesaid adaptive ICI based algorithm is used to calculate the maximal  $h_k$  which provides an optimal trade-off between the estimation error variance and the bias. In simple terms, a proper  $\Gamma$  value ensures selecting the largest vicinity neighbouring the considered signal sample (such that the LPA fits well to data) which results in an optimal noise smoothing effect [10]. To justify the previous assertion, let us consider the LPA estimation error calculated as:

$$e_{h_k}(n) = |y(n) - \hat{y}_{h_k}(n)|, \quad (8)$$

where  $y(n)$  stands for a noise-free signal sample and  $\hat{y}_{h_k}(n)$  represents its LPA estimate. The estimation error can be written as a sum of the bias and zero-mean random error [10]:

$$e_{h_k}(n) = b_{h_k}(n) + e_{h_k}^0(n). \quad (9)$$

Therefore, the following inequality is true [10]:

$$e_{h_k}(n) \leq |\bar{b}_{h_k}(n)| + |e_{h_k}^0(n)|, \quad (10)$$

where  $|\bar{b}_{h_k}(n)|$  represents the maximal value of  $|b_{h_k}(n)|$  and  $e_{h_k}^0(n)$  is, in case of the Gaussian noise, zero-mean estimation error with standard deviation  $\sigma_{h_k}(n)$ .

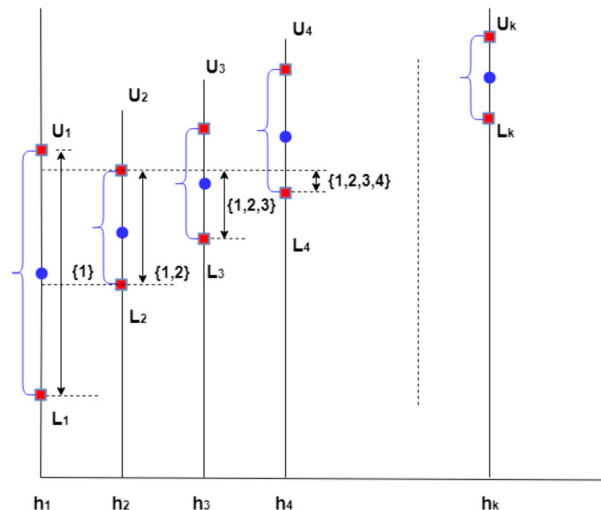


**Figure 1.** Illustration of the ICI rule tracking the intersection of confidence intervals.

Additionally, the following inequality holds true with probability  $p = 1 - \alpha$ :

$$|e_{h_k}^0(n)| \leq \chi_{1-\alpha/2} \cdot \sigma_{h_k}(n), \quad (11)$$

where  $1 - \alpha/2$  stands for  $(1 - \alpha/2)$ -th quantile of the normal distribution  $\mathcal{N}(0, 1)$  [10]. In other words, the estimation error  $e_{h_k}^0(n)$  is found inside the interval

$[-\chi_{1-\alpha/2} + \chi_{1-\alpha/2}]$  with the probability  $p$ . Based on the Equations (10) and (11), it follows that [10]:

$$|e_{h_k}(n)| \leq |\bar{b}_{h_k}(n)| + \chi_{1-\alpha/2} \cdot \sigma_{h_k}(n) \quad (12)$$

holds true with the same probability  $p = 1 - \alpha$  [10]. The optimal  $h_k$ , denoted as  $h^*$ , is chosen as the one providing optimal estimation error bias to the variance trade-off, such that  $h_k \leq h^*$ . Hence the following

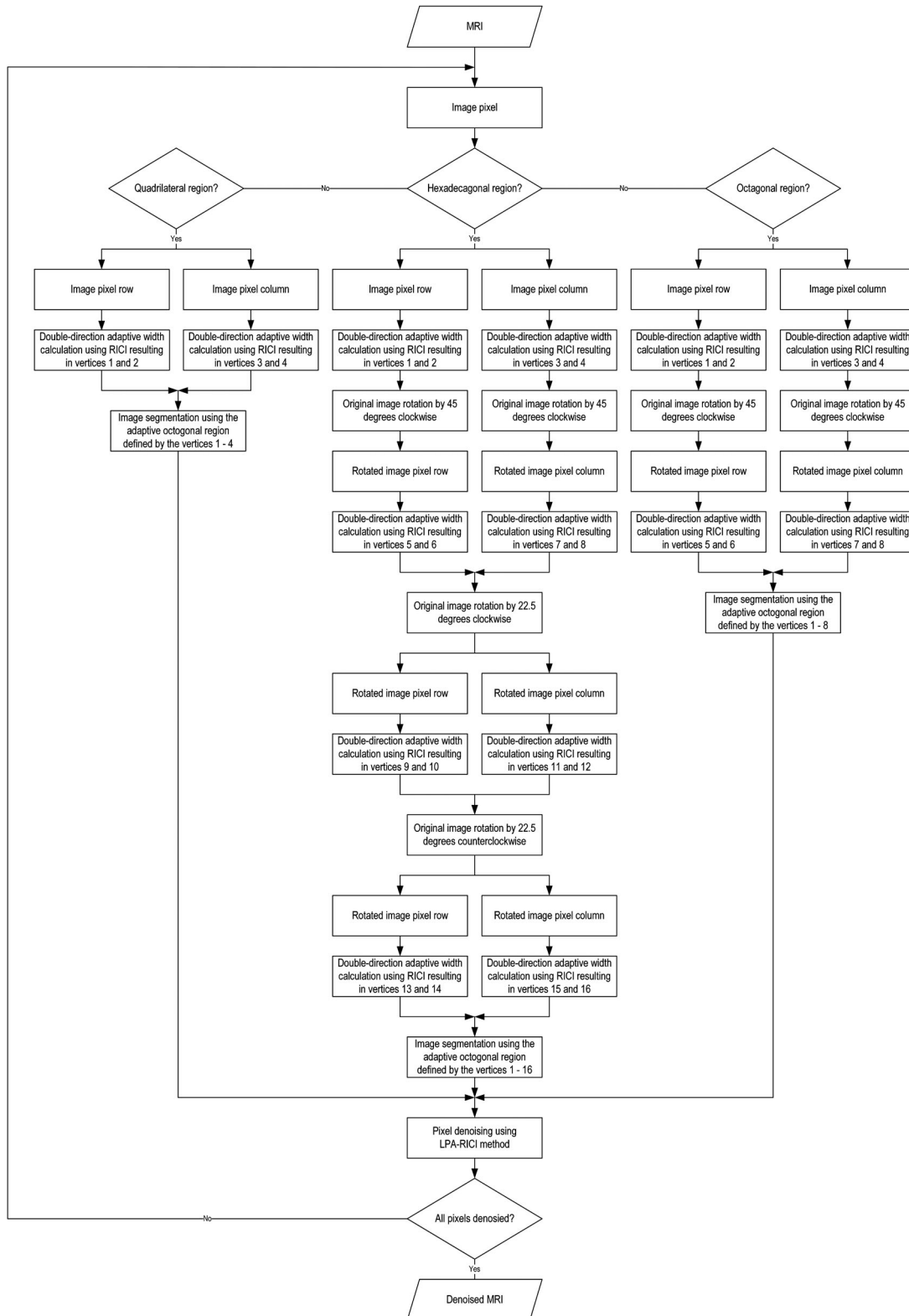


Figure 2. Flowchart of the proposed LPA-RICI based MRI denoising method.

expression is true [10]:

$$|e_{h_k}(n)| \leq \Gamma \cdot \sigma_{h_k}(n). \quad (13)$$

Consequently, the inequality (13) can be written as:

$$|y(n) - \hat{y}_{h_k}(n)| \leq \Gamma \cdot \sigma_{h_k}(n), \quad (14)$$

or as

$$\hat{y}_{h_k}(n) - \Gamma \cdot \sigma_{h_k}(n) \leq y(n) \leq \hat{y}_{h_k}(n) + \Gamma \cdot \sigma_{h_k}(n), \quad (15)$$

where  $\hat{y}_{h_k}(n) - \Gamma \cdot \sigma_{h_k}(n)$  stands for the lower confidence interval limit  $L_{h_k}(n)$  and  $\hat{y}_{h_k}(n) + \Gamma \cdot \sigma_{h_k}(n)$  for the upper confidence interval limit  $U_{h_k}(n)$ , as defined in Equations (3) and (4). Since both expressions Equations (11) and (14) are true with the same probability  $p$ , we can claim with that same probability that  $y(n)$  is within the interval  $\hat{y}_{h_k}(n) \pm \Gamma \cdot \sigma_{h_k}(n)$  for  $h_k \leq h^*$  [10]. In simple terms, nonempty intersection of all subsequent confidence intervals ensures  $h_k \leq h^*$ . On the other hand, if intersection of all previous confidence intervals is an empty set, it means that  $h_k > h^*$  [10]. Thereby, the largest  $h_k$  (as close to  $h^*$  as possible) is to be chosen as the one giving the near optimal balance between the estimation error variance and the bias, as required by the Equation (7).

An illustration of tracking the intersection of confidence intervals by the ICI rule is shown in Figure 1. As it can be seen, the first four confidence intervals have common points, i.e. their intersection is nonempty. Since the next confidence interval is not overlapping with all four of the previous confidence intervals, the ICI rule results in  $h_4$  being chosen as the proper estimator size.

### Improved ICI Rule

The performances of the ICI algorithm are highly affected by the chosen  $\Gamma$  value. Namely, too large  $\Gamma$  values result in signal oversmoothing (meaning that the noise is well removed but object edges are blurred). On the other hand, too small  $\Gamma$  values cause signal undersmoothing (i.e. significant amount of noise is left in the image) [8,9].

Hence, we introduce a modification of the ICI algorithm shown to be highly robust to suboptimal  $\Gamma$  selections [11–13]. The modified algorithm, called the RIC algorithm, was further extended to 2D denoising of MRI images. The proposed method tracks the amount of overlapping of all previous confidence intervals

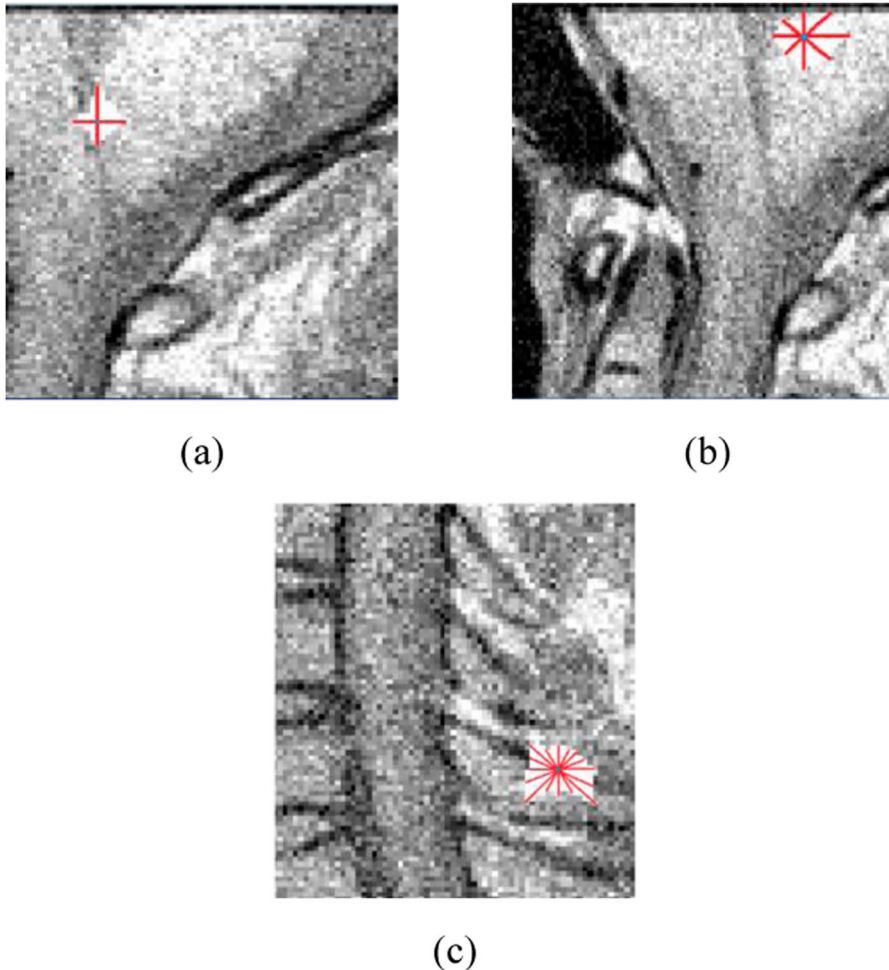


**Figure 3.** Examples of the regions calculated by the proposed 2D LPA-RICI method. (a) Quadrilateral region. (b) Octagonal region. (c) Hexadecagonal region.

and with respect to the length of the current confidence interval, defined as [11–13]:

$$R_{h_k}(n) = \frac{U_{h_k}(n) - \bar{L}_{h_k}(n)}{U_{h_k}(n) - L_{h_k}(n)}. \quad (16)$$

It is then used as an additional criterion for selecting the proper estimator size, such that [11–13]:

$$R_{h_k}(n) \geq R_c, \quad (17)$$

where  $R_c$  denotes the preset data-driven threshold [11]. In other words, unlike the ICI algorithm which requires just the existence of the overlapping of the confidence intervals, the proposed RICl based algorithm requires a certain percentage of overlapping

(defined by the Equation (17)). Owing to this additional requirement, the RICl algorithm allows selecting larger  $\Gamma$  values (ensuring efficient noise removal) while additional criterion given in Equation (17) prevents from blurring artefacts and ensures object edge and contour preserving.

#### ICI and RICl rule in image processing

Also, here we propose upgrading the original ICI algorithm and its improved version (the RICl algorithm), defined for 1D signal processing, to 2D image processing. Namely, instead of detecting the adaptive data-driven sequence of likely samples

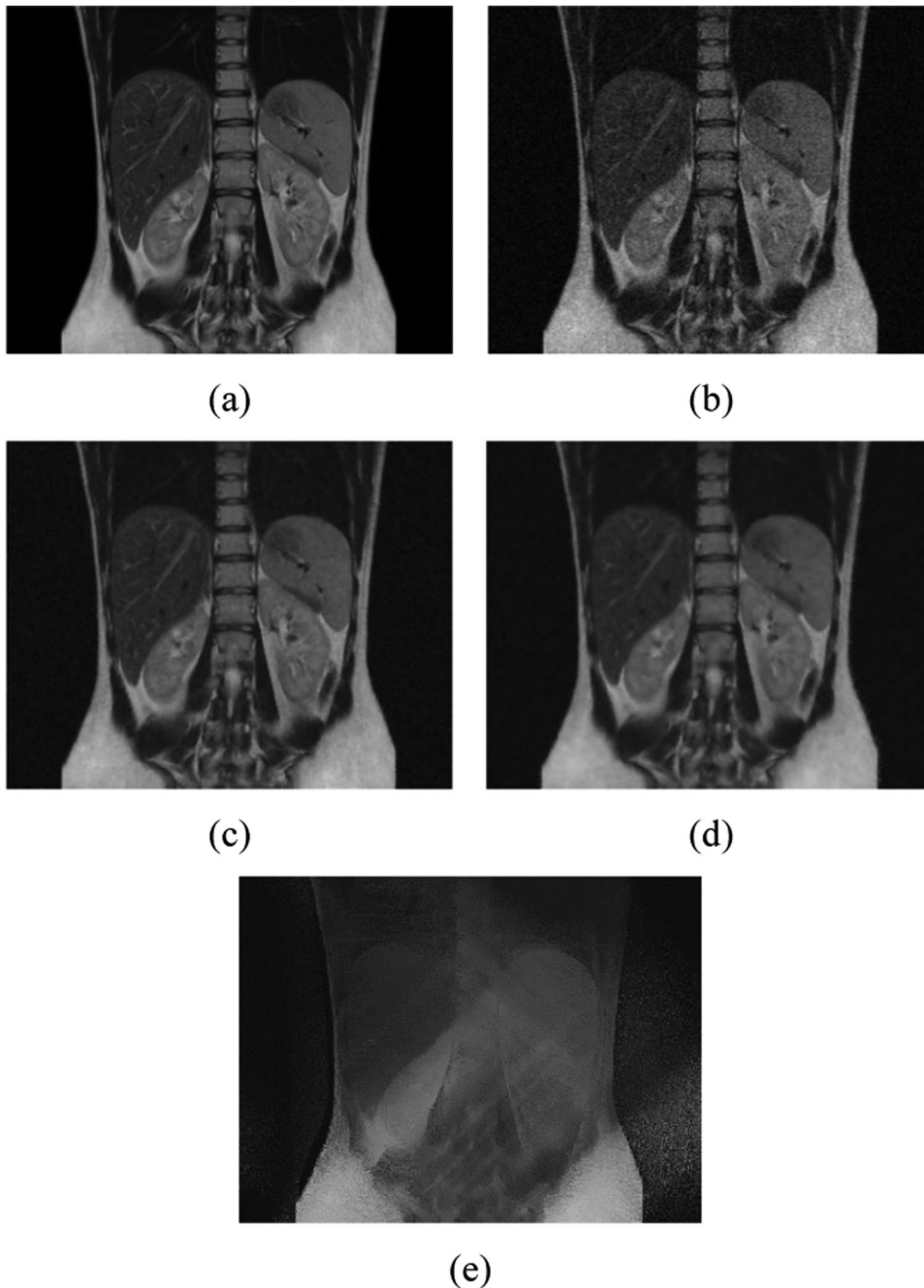


**Figure 4.** Abdomen MRI scan. (a) Original noise-free image. (b) Noisy image (AWGN with  $\sigma = 25$ ). (c) Image denoised using the LPA-RICl method (quadrilateral region,  $\Gamma = 1.7$ ,  $R_c = 0.9$ ). (d) Image denoised using the LPA-RICl method (octagonal region,  $\Gamma = 1.7$ ,  $R_c = 0.9$ ). (e) Image denoised using the LPA-RICl method (hexadecagonal region,  $\Gamma = 1.7$ ,  $R_c = 0.9$ ).

**Table 1.** PSNRs of the abdomen MRI denoised using the LPA-ICI method, LPA-RICI method and fixed size filtering (best results are marked in bold).

Region	$\Gamma$	$R_c$	$\sigma$	PSNR [dB]			
				Noisy image	Fixed	ICI	RICI
Quad.	1.7	0.9	20	31.12	32.40	36.51	37.24
Octa.	1.7	0.9	20	31.12	32.40	35.51	36.41
Hexa.	1.7	0.9	20	31.12	32.40	32.51	32.70
Quad.	1.7	0.9	25	30.65	32.11	36.29	36.97
Octa.	1.7	0.9	25	30.65	32.11	35.20	36.28
Hexa.	1.7	0.9	25	30.65	32.11	32.61	32.83
Quad.	1.7	0.9	30	30.34	31.74	36.34	36.82
Octa.	1.7	0.9	30	30.34	31.74	35.12	36.30
Hexa.	1.7	0.9	30	30.34	31.74	32.74	33.01
Quad.	1.6	0.6	20	31.12	32.40	36.66	<b>37.26</b>
Octa.	1.6	0.6	20	31.12	32.40	35.48	36.31
Hexa.	1.6	0.6	20	31.12	32.40	32.53	32.83
Quad.	1.6	0.6	25	30.65	32.11	36.42	36.93
Octa.	1.6	0.6	25	30.65	32.11	35.27	36.31
Hexa.	1.6	0.6	25	30.65	32.11	32.64	32.83
Quad.	1.6	0.6	30	30.34	31.74	36.14	36.75
Octa.	1.6	0.6	30	30.34	31.74	35.26	<b>36.58</b>
Hexa.	1.6	0.6	30	30.34	31.74	32.79	32.91
Quad.	1.5	0.8	20	31.12	32.40	36.78	37.16
Octa.	1.5	0.8	20	31.12	32.40	35.65	36.56
Hexa.	1.5	0.8	20	31.12	32.40	32.57	32.74
Quad.	1.5	0.8	25	30.65	32.11	36.51	36.92
Octa.	1.5	0.8	25	30.65	32.11	35.48	36.36
Hexa.	1.5	0.8	25	30.65	32.11	32.67	32.83
Quad.	1.5	0.8	30	30.34	31.74	36.45	36.69
Octa.	1.5	0.8	30	30.34	31.74	35.44	36.37
Hexa.	1.5	0.8	30	30.34	31.74	32.81	<b>33.03</b>

neighbouring the considered sample in 1D signals, we propose detecting the adaptive data-driven 2D regions of likely pixels in vicinity of the analysed pixel (as shown in the methods flowchart given in Figure 2).

In order to do so, the upper and lower interval limits  $U_{h_k}(n)$  and  $L_{h_k}(n)$ , defined in Equations (3) and (4), are

extended to  $U_{h_k}(i, j)$  and  $L_{h_k}(i, j)$  for the purpose of image processing, where  $i$  and  $j$  stand for image pixel indices.

Thus, the adaptive 2D regions (varying in size and shape from pixel to pixel depending on image content) are obtained and utilized to form masks for image segmentation and extraction of the region of interest in vicinity of the considered pixel.

Next, denoised pixel value is estimated using the 2D LPA based weighted averaging of the pixels in the detected region. The same procedure is repeated for each image pixel separately. Note also that this is one of the important advantages of the proposed method, since the 2D LPA-RICI algorithm is an excellent candidate for parallelized implementation in order to improve its computational efficiency.

The size of the adaptive 2D regions used in this paper was calculated based on the two, four and eight lines which form quadrilateral, octagonal and hexadecagonal regions, respectively. An example of each region is given in Figure 3.

The obtained results using both 2D LPA-ICI and 2D LPA-RICI methods are presented in the next section.

## Results

The proposed adaptive 2D LPA-RICI method was applied to two test MRI images (an abdomen and a knee MRI) and compared to adaptive 2D LPA-ICI and fixed size filtering methods. The obtained results were compared in terms of the peak signal-to-noise ratio (PSNR).

**Table 2.** Comparison of the PSNRs for abdomen MRI denoised by the 2D LPA-ICI, 2D LPA-RICI and fixed size filtering methods.

Region	$\Gamma   R_c   \sigma$	PSNR [dB]					
		Fixed vs. noisy	ICI vs. noisy	RICI vs. noisy	ICI vs. fixed	RICI vs. fixed	RICI vs. ICI
Quad.	1.7 0.9 20	1.28	5.39	6.12	4.11	4.84	0.73
Octa.	1.7 0.9 20	1.28	4.39	5.29	3.11	4.01	0.9
Hexa.	1.7 0.9 20	1.28	1.39	1.42	0.11	0.14	0.03
Quad.	1.7 0.9 25	1.46	5.64	6.32	4.18	4.86	0.68
Octa.	1.7 0.9 25	1.46	4.55	5.63	3.09	4.17	1.08
Hexa.	1.7 0.9 25	1.46	1.96	2.02	0.5	0.56	0.06
Quad.	1.7 0.9 30	1.4	6	6.48	4.6	5.08	0.48
Octa.	1.7 0.9 30	1.4	4.78	5.96	3.38	4.56	1.18
Hexa.	1.7 0.9 30	1.4	2.4	2.51	1	1.11	0.11
Quad.	1.6 0.6 20	1.28	5.54	6.14	4.26	4.86	0.6
Octa.	1.6 0.6 20	1.28	4.36	5.19	3.08	3.91	0.83
Hexa.	1.6 0.6 20	1.28	1.41	1.55	0.13	0.27	0.14
Quad.	1.6 0.6 25	1.46	5.77	6.28	4.31	4.82	0.51
Octa.	1.6 0.6 25	1.46	4.62	5.66	3.16	4.2	1.04
Hexa.	1.6 0.6 25	1.46	1.99	2.05	0.53	0.59	0.06
Quad.	1.6 0.6 30	1.4	5.8	6.41	4.4	5.01	0.61
Octa.	1.6 0.6 30	1.4	4.92	6.24	3.52	4.84	1.32
Hexa.	1.6 0.6 30	1.4	2.45	2.49	1.05	1.09	0.04
Quad.	1.5 0.8 20	1.28	5.66	6.04	4.38	4.76	0.38
Octa.	1.5 0.8 20	1.28	4.53	5.44	3.25	4.16	0.91
Hexa.	1.5 0.8 20	1.28	1.45	1.53	0.17	0.25	0.08
Quad.	1.5 0.8 25	1.46	5.86	6.27	4.4	4.81	0.41
Octa.	1.5 0.8 25	1.46	4.83	5.71	3.37	4.25	0.88
Hexa.	1.5 0.8 25	1.46	2.02	2.05	0.56	0.59	0.03
Quad.	1.5 0.8 30	1.4	6.11	6.35	4.71	4.95	0.24
Octa.	1.5 0.8 30	1.4	5.1	6.03	3.7	4.63	0.93
Hexa.	1.5 0.8 30	1.4	2.47	2.77	1.07	1.37	0.3

The noise-free abdomen MRI image (with resolution  $960 \times 720$ ) is given in Figure 4(a). Next, noisy image corrupted by the additive white Gaussian noise (AWGN) with standard deviation  $\sigma = 25$  is shown in Figure 4 (b). Figure 4(c, d and e) present images denoised using the algorithm based on the RICl method. Namely, Figure 4(c) is obtained using the quadrilateral

regions, Figure 4(d) is obtained using the octagonal regions, and Figure 4(e) is obtained using the hexadecagonal regions.

The results for denoised abdomen MRI images, in terms of the PSNR, are shown in Table 1 with respect to various  $\Gamma$  and  $R_c$  values for different noise levels. The first column of the table provides the regions

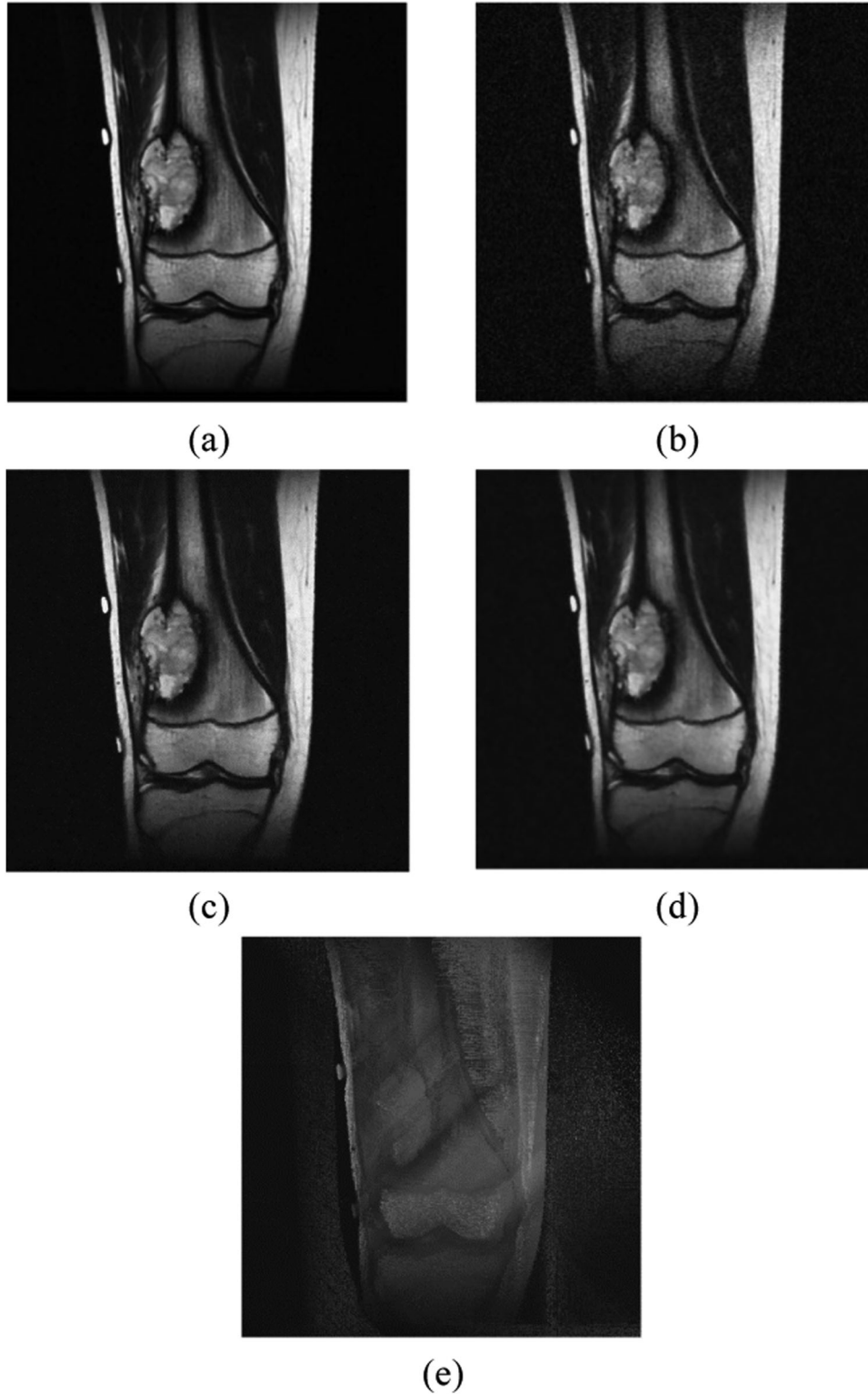


**Figure 5.** Knee MRI scan. (a) Original noise-free image. (b) Noisy image (AWGN with  $\sigma = 25$ ). (c) Image denoised using the LPA-RICl method (quadrilateral region,  $\Gamma = 1.7$ ,  $R_c = 0.9$ ). (d) Image denoised using the LPA-RICl method (octagonal region,  $\Gamma = 1.7$ ,  $R_c = 0.9$ ). (e) Image denoised using the LPA-RICl method (hexadecagonal region,  $\Gamma = 1.7$ ,  $R_c = 0.9$ ).

**Table 3.** PSNRs of the knee MRI denoised using the LPA-ICI method, LPA-RICI method and fixed size filtering.

Region	$\Gamma$	$R_c$	$\sigma$	PSNR [dB]			
				Noisy image	Fixed	ICI	RICI
Quad.	1.7	0.9	20	31.56	32.92	38.33	39.19
Octa.	1.7	0.9	20	31.56	32.92	36.83	38.03
Hexa.	1.7	0.9	20	31.56	32.92	33.32	33.42
Quad.	1.7	0.9	25	31.14	32.87	37.95	38.73
Octa.	1.7	0.9	25	31.14	32.87	36.57	37.75
Hexa.	1.7	0.9	25	31.14	32.87	33.34	33.58
Quad.	1.7	0.9	30	30.84	31.93	37.57	38.24
Octa.	1.7	0.9	30	30.84	31.93	36.38	37.51
Hexa.	1.7	0.9	30	30.84	31.93	33.4	33.71
Quad.	1.6	0.6	20	31.56	32.92	38.49	<b>39.31</b>
Octa.	1.6	0.6	20	31.56	32.92	37.03	38.2
Hexa.	1.6	0.6	20	31.56	32.92	33.35	33.64
Quad.	1.6	0.6	25	31.14	32.87	38.02	38.68
Octa.	1.6	0.6	25	31.14	32.87	36.77	37.85
Hexa.	1.6	0.6	25	31.14	32.87	33.4	33.8
Quad.	1.6	0.6	30	30.84	31.93	37.79	38.41
Octa.	1.6	0.6	30	30.84	31.93	36.52	37.63
Hexa.	1.6	0.6	30	30.84	31.93	33.43	33.74
Quad.	1.5	0.8	20	31.56	32.92	38.67	39.03
Octa.	1.5	0.8	20	31.56	32.92	37.19	<b>38.28</b>
Hexa.	1.5	0.8	20	31.56	32.92	33.36	33.64
Quad.	1.5	0.8	25	31.14	32.87	38.18	38.75
Octa.	1.5	0.8	25	31.14	32.87	36.91	37.87
Hexa.	1.5	0.8	25	31.14	32.87	33.41	33.85
Quad.	1.5	0.8	30	30.84	31.93	37.82	38.39
Octa.	1.5	0.8	30	30.84	31.93	36.67	37.67
Hexa.	1.5	0.8	30	30.84	31.93	33.48	<b>33.91</b>

(quadrilateral, octagonal or hexadecagonal) followed by the second and the third column rendering parameters  $\Gamma$  and  $R_c$  used in denoising by the proposed 2D LPA-RICI. The fourth column represents standard deviations of AWGN followed by the fifth column which provides the PSNR of the noisy image. The sixth column gives the PSNR of the MRI image denoised using the fixed size filtering. The last two columns render the PSNR of

images denoised using the ICI based method and the RICI based method, respectively.

Table 2 provides the comparison of the 2D LPA-ICI, 2D LPA-ICI and fixed size filtering for the abdomen MRI. As it can be seen, both ICI and RICI based are significantly more efficient than denoising based on the fixed size filtering. Namely, the fixed size filtering improved image PSNR by up to 1.46 dB when compared to the noisy image. On the other hand, 2D LPA-ICI filtering increased the PSNR of the denoised MRI image by up to 6.11 dB, while its modification (2D LPA-RICI method) improved the PSNR by up to 6.48 dB. Thus, the adaptive method based on the RICI algorithm has significantly improved denoised image quality both in terms of the PSNR and visually (as it can be seen in Figure 4). Furthermore, the ICI based adaptive filtering outperformed the fixed size filtering by up to 4.71 dB. On the other hand, the RICI based adaptive method outperformed the fixed size filtering up to 5.08 dB.

The knee MRI images (resolution of which is  $1024 \times 1024$ ) are shown in Figure 5. Figure 5(a) shows the original noise-free MRI image, followed by Figure 5(b) showing the noisy image corrupted by the AWGN with standard deviation  $\sigma = 25$ . Figure 5(c), 5(d) and 5(e) present the denoised images obtained using the 2D LPA-RICI method with quadrilateral, octagonal and hexadecagonal regions, respectively.

Denoising results for knee MRI images are presented in Table 3. As for the abdomen MRI, the adaptive ICI and RICI based methods significantly outperformed the fixed size filtering. Furthermore, the RICI based method also outperformed the ICI based method.

**Table 4.** Comparison of the PSNRs for knee MRI denoised by the 2D LPA-ICI, 2D LPA-RICI and fixed size filtering methods.

Region	$\Gamma   R_c   \sigma$	PSNR [dB]					
		Fixed vs. noisy	ICI vs. noisy	RICI vs. noisy	ICI vs. fixed	RICI vs. fixed	RICI vs. ICI
Quad.	1.7 0.9 20	1.36	6.77	7.63	5.41	6.27	0.86
Octa.	1.7 0.9 20	1.36	5.27	6.47	3.91	5.11	1.2
Hexa.	1.7 0.9 20	1.36	1.76	1.86	0.4	0.5	0.1
Quad.	1.7 0.9 25	1.73	6.81	7.59	5.08	5.86	0.78
Octa.	1.7 0.9 25	1.73	5.43	6.61	3.7	4.88	1.18
Hexa.	1.7 0.9 25	1.73	2.2	2.44	0.47	0.71	0.24
Quad.	1.7 0.9 30	1.09	6.73	7.4	5.64	6.31	0.67
Octa.	1.7 0.9 30	1.09	5.54	6.67	4.45	5.58	1.13
Hexa.	1.7 0.9 30	1.09	2.56	2.87	1.47	1.78	0.31
Quad.	1.6 0.6 20	1.36	6.93	7.75	5.57	6.39	0.82
Octa.	1.6 0.6 20	1.36	5.47	6.64	4.11	5.28	1.17
Hexa.	1.6 0.6 20	1.36	1.79	2.08	0.43	0.72	0.29
Quad.	1.6 0.6 25	1.73	6.88	7.54	5.15	5.81	0.66
Octa.	1.6 0.6 25	1.73	5.63	6.71	3.9	4.98	1.08
Hexa.	1.6 0.6 25	1.73	2.26	2.66	0.53	0.93	0.4
Quad.	1.6 0.6 30	1.09	6.95	7.57	5.86	6.48	0.62
Octa.	1.6 0.6 30	1.09	5.68	6.79	4.59	5.7	1.11
Hexa.	1.6 0.6 30	1.09	2.59	2.9	1.5	1.81	0.31
Quad.	1.5 0.8 20	1.36	7.11	7.47	5.75	6.11	0.36
Octa.	1.5 0.8 20	1.36	5.63	6.72	4.27	5.36	1.09
Hexa.	1.5 0.8 20	1.36	1.8	2.08	0.44	0.72	0.28
Quad.	1.5 0.8 25	1.73	7.04	7.61	5.31	5.88	0.57
Octa.	1.5 0.8 25	1.73	5.77	6.73	4.04	5	0.96
Hexa.	1.5 0.8 25	1.73	2.27	2.71	0.54	0.98	0.44
Quad.	1.5 0.8 30	1.09	6.98	7.55	5.89	6.46	0.57
Octa.	1.5 0.8 30	1.09	5.83	6.83	4.74	5.74	1
Hexa.	1.5 0.8 30	1.09	2.64	3.07	1.55	1.98	0.43

A comparison of the obtained results for knee MRI images is given in Table 4. The first three columns in Table 4 give an increase in the PSNR when compared to the noisy image for fixed size filtering, the ICI based method and the RICl based method, respectively. Namely, the fixed size filtering increased the denoised MRI image PSNR by up to 1.73 dB, the 2D LPA-ICI filtering increased the PSNR by up to 7.11 dB and the adaptive 2D LPA-RICl based filtering increased the denoised PSNR by up to 7.75 dB, when compared to the noisy image. Furthermore, the ICI based filtering outperformed the fixed size filtering by up to 5.89 dB. On the other hand, the 2D LPA-RICl filtering outperformed the 2D LPA-ICI filtering by up to 1.20 dB.

The results given in Tables 1–4 show that the proposed 2D LPA-RICl based method is a powerful tool for MRI image denoising, significantly outperforming fixed size filtering. Furthermore, it was also shown that the proposed modification of the ICI based method (called 2D LPA-RICl) outperforms the original 2D LPA-ICI for all tested MRI images and noise levels.

Also, it is important to note that the larger number of the polygonal angles in adaptive 2D regions used in the adaptive ICI and RICl based algorithms does not necessarily result in significant improvements in the MRI image denoising results.

In addition, since denoising each image pixel is done independently, the method is easy to parallelize in order to reduce its execution time.

## Conclusion

An adaptive method for MRI image denoising was proposed in the paper. The method is based on a modification of the ICI algorithm called the RICl algorithm. The RICl algorithm was further extended to 2D image denoising. The 2D LPA-ICI method was shown to increase PSNRs of denoised MRI images by up to 7.11 dB when compared to noisy images outperforming fixed size filtering by up to 5.89 dB. In contrast, the 2D LPA-RICl method was shown to increase PSNRs of denoised MRI images by up to 7.75 dB when compared to the noisy image, outperforming the 2D LPA-ICI method by up to 1.32 dB and fixed size filtering by up to 6.48 dB. This improvement is caused by calculating the size and shape of 2D regions locally and independently for each image pixel. Thus, the method is easy to parallelize in order to reduce its execution time. Furthermore, three types of the adaptive regions (quadrilateral, octagonal and hexadecagonal) were tested showing that the larger number of polygonal angles in adaptive 2D regions does not necessarily lead to significant improvements in image denoising quality. However, for all three types of regions and all tested noise levels, the 2D LPA-RICl method outperformed other tested methods (fixed size filtering and the adaptive ICI based method).

## Disclosure statement

No potential conflict of interest was reported by the authors.

## Notes on contributors

**Jonatan Lerga**, Head of the Laboratory for Application of Information Technologies at the Faculty of Engineering, University of Rijeka, Croatia, received his MS degree in Electrical Engineering from the Faculty of Engineering, University of Rijeka, in 2006, and the PhD degree from the Faculty of Electrical Engineering and Computing, University of Zagreb, Croatia in 2011. Since 2007, he has been with the Faculty of Engineering, University of Rijeka. In 2012, he received the Award of the Croatian Academy of Engineering for his scientific achievements, as well as the annual award of the City of Rijeka in 2015 and annual award of the Primorje-Gorski Kotar County in 2018. He also received annual awards from the Foundation of the University of Rijeka in 2008 and 2010. His main research interests are statistical signal processing, time-frequency signal analysis, image and video processing, and biomedical signal processing.

**Ivica Mandić**, Information System Developer at Hrvatski telekom, received his Master's degree in Computing from the Faculty of Engineering, University of Rijeka, Croatia, in April 2018. Since 2017, he worked as Software Developer for desktop applications used in maritime affairs. Following that, since 2018, he has been with Hrvatski Telekom, a company in the Deutsche Telekom group, as Information System Developer.

**Hajdi Peić**, former student at the Faculty of Engineering, University of Rijeka, Croatia, received her master's degree in Computing from the Faculty of Engineering, University of Rijeka, in April 2018. Since then, she has been a part of the team in one of the Kirey Group companies with branch office in Rijeka, Croatia, taking the position of the software application tester.

**Drazen Brščić** received his BSc and MSc degrees in electrical engineering from the University of Zagreb, Croatia, in 2000 and 2004, respectively, and the Dr. Eng. degree in electrical engineering from The University of Tokyo, Japan in 2008. From 2008 to 2010 he worked as a postdoctoral researcher at the Technische Universität München, Germany. In 2011 he joined ATR Intelligent Robotics and Communication Laboratories in Kyoto, Japan, as research scientist. Since 2016 he is working as a assistant professor at the Faculty of Engineering, University of Rijeka. His research interests include person tracking, mobile robotics and human-robot interaction.

## ORCID

Jonatan Lerga  <http://orcid.org/0000-0002-4058-8449>

## References

- [1] Ciulla C. Improved signal and image interpolation in biomedical applications: the case of magnetic resonance imaging (MRI). Information science reference, New York, USA: Hershey; 2009.
- [2] Caverly RH. MRI fundamentals: RF aspects of magnetic resonance imaging (MRI). IEEE Microw Mag. 2015;16(6):20–33.
- [3] Bibb R, Eggbeer D, Paterson AM. Medical modelling: the application of advanced design and rapid prototyping techniques in medicine. Woodhead Publishing, 2015.

- [4] Sprawls P. The physical principles of medical imaging. Madison (WI): Medical Physics Pub Corp. 1995.
- [5] Vaishali S, Rao KK, Rao GVS. A review on noise reduction methods for brain MRI images. 2015 International Conference on Signal Processing and Communication Engineering Systems; Guntur; 2015. p. 363–365.
- [6] Anand CS, Sahambi JS. MRI denoising using bilateral filter in redundant wavelet domain. TENCON 2008–2008 IEEE Region 10 Conference; 2008 November. p. 1–6.
- [7] Saha PK, Udupa JK. Scale-based diffusive image filtering preserving boundary sharpness and fine structures. IEEE Trans Med Imaging. 2001;20(11):1140–1155.
- [8] Katkovnik V, Egiazarian K, Astola J. A spatially adaptive nonparametric regression image deblurring. IEEE Trans Image Process. 2005;14(10):1469–1478.
- [9] Katkovnik V, Egiazarian K, Astola J. Adaptive window size image denoising based on intersection of confidence intervals (ICI) rule. J Math Imaging Vis. 2002;16(3):223–235.
- [10] Katkovnik V, Egiazarian K, Astola J. Local approximation techniques in signal and image processing. Washington (DC): SPIE Press; 2016.
- [11] Lerga J, Vrankic M, Sucic V. A signal denoising method based on the improved ICI rule. IEEE Signal Process Lett. 2008;15:601–604.
- [12] Lerga J, Sucic V, Grbac E. An adaptive method for video denoising based on the ICI rule. Eng Rev. 2012;32(1):33–40.
- [13] Segon G, Lerga J, Sucic V. Improved LPA-ICI-based estimators embedded in a signal denoising virtual instrument. Signal ImageVideo Process. 2016;2016:1–8.